Measurement of dielectron production in niobium-niobium collisions at 1.05 GeV/nucleon

S. Beedoe,[1,5],* J. Carroll,[1] P. Force,[2] J. Gordon,[1],† T. Hallman,[3] G. Igo,[1] P. N. Kirk,[4] G. Krebs,[5] A. Letessier-Selvon,[5],‡ L. Madansky,[3] H. S. Matis,[5] D. Miller,[6] C. Naudet,[5] G. Roche,[2,5] L. S. Schroeder,[5] P. Seidl,[5] Z. F. Wang,[4] R. Welsh,[3] and A. Yegneswaran[7]

[1] *University of California at Los Angeles, Los Angeles, California 90024*
[2] *Université Blaise Pascal/Institut National de Physique Nucléaire et de Physique des Particules, 63177 Aubière Cedex, France*
[3] *The Johns Hopkins University, Baltimore, Maryland 21218*
[4] *Louisiana State University, Baton Rouge, Louisiana 70803*
[5] *Lawrence Berkeley Laboratory, University of California, Berkeley, California 94720*
[6] *Northwestern University, Evanston, Illinois 60201*
[7] *Continuous Electron Beam Accelerator Facility, Newport News, Virginia 23606*

(Received 11 February 1992)

A dielectron signal for pair masses greater than M_π is observed in Nb+Nb collisions at 1.05 GeV/nucleon beam kinetic energy. The invariant mass spectrum and the associated multiplicity distribution are presented. Comparisons are made with previous cross section measurements in p+Be and Ca+Ca.

PACS number(s): 25.75.+r

I. INTRODUCTION

Collisions between relativistic nuclei offer the opportunity to study hadronic interactions in an excited multihadron environment. By studying such collisions it may be possible to obtain information about the nuclear equation of state in new domains of temperature and pressure [1–4]. Virtual photons are produced in these collisions by particle interactions and decays, and are detected as lepton pairs. The lepton pairs, in contrast to hadronic probes, have only a small final state interaction and thus provide direct information about the conditions at production of the virtual photon. Electron pairs that result from pion annihilation may provide a means for studying pion dynamics in excited nuclear matter [5, 6]. In this paper, we present results of dielectron production in Nb+Nb collisions at 1.05 GeV/nucleon. These data represent the heaviest colliding system for which dielectron production has been measured and are the first for which the associated multiplicity spectrum is available.

An overview of the apparatus used to measure the dielectron cross sections is given in Sec. II. Section III contains a discussion of the data analysis and the results of a study of the effects of large multiplicities on the efficiency and resolution of the combined detector and analysis systems. In Sec. IV we show the results of our measurements and compare them with previous data and theoretical calculations.

II. EXPERIMENTAL SETUP

These measurements were made at the Lawrence Berkeley Laboratory Bevalac using the Dilepton Spectrometer (DLS) [7,8] with an added 96-element multiplicity detector (see Fig. 1 in Ref. [8]), which surrounded the target. Each of the two symmetric arms of the spectrometer, which were centered at 40° with respect to the beam axis, contained a large acceptance dipole magnet, two scintillator hodoscopes for triggering and simple localization of charged particles, two segmented gas Cherenkov counters for electron identification, and three drift chambers for tracking particles. An additional x-measuring plane was added to each drift chamber stack in the spectrometer prior to this experiment to increase the resolution and overall tracking efficiency. Lead glass blocks located behind the scintillator hodoscope were used to check the hadron rejection power and electron efficiency of the Cherenkov counters. The dielectron trigger was an eightfold coincidence between the four scintillator hodoscopes and the four Cherenkov counters.

A cross section of the multiplicity array is shown in Fig. 1. It consists of 96 plastic scintillator pieces (0.32 cm thick); 48 each covering the region of the conical scattering chamber above (below) the thin windows through, which particles enter the spectrometer. The upper and lower halves are themselves each divided into two parts covering the polar angle ranges from 13° to 51.4° and 51.4° to 90°. Within each of these halves, 24 azimuthal strips cover angles from 13° to 167° and from 193° to 347°. The total angular acceptance subtended by the multiplicity array at the target is about 3.6 sr.

Monte Carlo studies, with the cascade code of Cugnon and co-workers [9], have shown that 98% of the particles detected by this array are either participant protons

*Now at Hampton University, Hampton, VA 23668.
†Now at Radiation Monitoring Devices, Inc., 44 Hunt Street, Watertown, MA 02172.
‡Now at Université de Paris VI et VII, LPNHE, 75730 Paris Cedex 05, France.

 ©1993 The American Physical Society

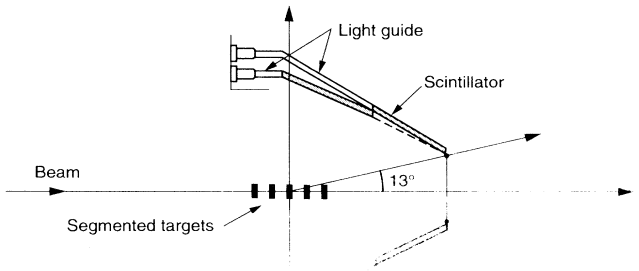

FIG. 1. Diagram of the multiplicity array: 48 scintillator elements are on the top half and 48 are on the bottom half of the conical scattering chamber.

or produced pions. Most target spectator fragments do not have enough energy to pass through the wall of the scattering chamber, and most projectile fragments are produced at forward angles outside of the array coverage.

III. DATA ANALYSIS AND MONTE CARLO STUDY

A. Analysis

Off-line analysis first reduces the data sample by requiring at least one electron quasitrack on each arm. An electron quasitrack is a first-order trajectory based upon the geometrical alignment of individual hodoscope and the Cherenkov elements that have produced acceptable signals. The following conditions are imposed to give a large probability that a quasitrack was an electron. First, the pulse heights in the hodoscopes and the Cherenkov counters, and the time of flight between the front and rear detector elements are all required to have values within optimized ranges corresponding to an electron traversing the system. Finally, the geometric pattern of the detectors with acceptable signals must correspond to a possible trajectory of an electron from the target with momentum greater than 50 MeV.

The electron quasitrack defines an area within each of the three drift chamber stacks which may contain information about an electron trajectory. Space points at the center of each stack were computed from the wire plane data in this area if sufficient information was available. (Good data from at least three planes were required.) Tracks and momentum vectors were constructed from the space points in the three stacks, and the tracks from the two arms were used to find pair vertices. Requirements on the goodness of fit in the full track reconstruction and on vertex quantities removed spurious tracks.

B. Background rejection

The probability for misidentification of a pion is $(1–3)\times10^{-3}$ per Cherenkov detector, about 5×10^{-6} per arm [10]. Since the estimated e/π ratio is of the order of 10^{-4}, the above rejection power is adequate. For protons, dE/dx and time-of-flight cuts reduce the probability of misidentification even further. However, when the track multiplicity per arm increases, hadron misidentification may occur because of insufficient segmentation of the detectors (in particular the front Cherenkov counter). This effect results in multiplicity dependent corrections.

As discussed in our previous papers [7,8], the opposite-sign pair sample $N_{\rm OS}$ contains a number of false (combinatoric) pairs (F) equal to the number of like-sign pair $N_{\rm LS}$. Thus the true pair signal is obtained as $T = N_{\rm OS} - N_{\rm LS}$. The ratio of true to false pairs, R, is a measure of the combinatoric backgrounds in the experiment. The statistical significance of the true pair signal is given by

$$\frac{T}{\sigma_T} = \frac{N_{\rm OS} - N_{\rm LS}}{\sqrt{N_{\rm OS} + N_{\rm LS}}} = \sqrt{\frac{T}{1 + 2/R}}, \tag{1}$$

where σ_T is the statistical error in the number of true pairs due to the subtraction. The tracking and quasi-tracking cuts were chosen to maximize this ratio.

The main source of electrons/positrons that generates false pairs is π^0 decay, either directly through the Dalitz decay channel or through the external conversion of the real photons (Bethe-Heitler process). Both Dalitz and Bethe-Heitler electron pairs have small opening angles and are likely to give a signal in a single detector element before they enter the magnet. We have determined that the most efficient condition to optimize acceptance of true pairs and rejection of background is a cut on the calibrated front hodoscope pulse height. The result of this cut, however, is sensitive to charged particle multiplicity.

C. Simulation of detector response in high multiplicity environment

In Nb+Nb collisions at 1.05 GeV/nucleon, the average number of elements hit in the front and rear hodoscopes of each DLS arm is about five. The performance of the detector and the analysis procedures in the presence of these high hadron multiplicities was studied using a Monte Carlo method. The intranuclear cascade code developed by Cugnon and collaborators [9, 11] was used to generate hadron events from Nb+Nb collisions at 1.05 GeV/nucleon. Electron pair events were generated with kinematic distributions similar to p+Be data [12]. The momentum vectors from a generated electron pair were added to a list of particle momenta from a Nb+Nb cascade event and these mixed events were then propagated through the DLS GEANT simulation code accounting for multiple scattering, bremsstrahlung, energy loss, and particle decay. The code includes the detailed geometry of the spectrometer, as well as thicknesses of materials, such as the drift chamber walls, Cherenkov mirrors, the surrounding air, etc. The DLS dielectron trigger condition requires appropriate front and rear Cherenkov responses and appropriate energy deposition in the front and rear hodoscopes of each arm. For events that satisfied the trigger condition, the responses of the various detector elements were digitized, and the simulated data were then passed through the DLS analysis code. The

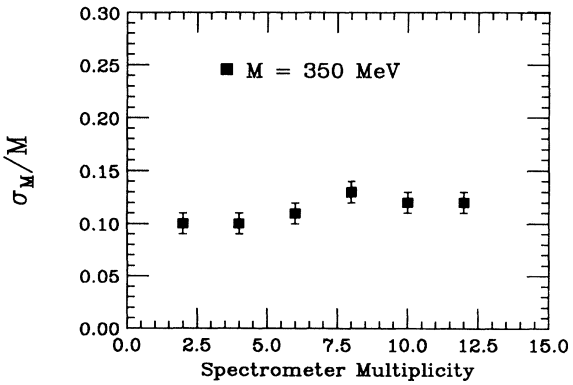

FIG. 2. Fractional mass resolution vs spectrometer multiplicity at fixed mass $M = 350$ MeV.

resolution and efficiency obtained in this way contain the effects of the analysis procedures as well as those of the detector itself [13].

For a fixed mass, $M = 350$ MeV, the mass resolution (σ/M) obtained from a Gaussian fit to the results described above, is plotted in Fig. 2 as a function of charged particle multiplicity $(N_{\rm sp})$ in the two spectrometer arms. This spectrometer multiplicity includes the two electrons that make up the trigger and those hadrons from the cascade calculation that enter the spectrometer arms [9]. The mass resolution shows little or no dependence on $(N_{\rm sp})$ and is never larger than 12% RMS.

The total efficiency (ϵ_T) of the analysis method is given by $\epsilon_T = \epsilon_{\rm qt}\epsilon_{\rm tr}$, where $\epsilon_{\rm qt}$ and $\epsilon_{\rm tr}$ are the quasitracking and tracking efficiencies, respectively. Quasitracking efficiency represents the loss of events due to cuts on the calibrated pulse heights and time of flights for the Cherenkov and hodoscope counters. Insufficient drift chamber information, noise, and resolution effects contribute to tracking inefficiency.

In order to estimate correctly the effect of high-multiplicity events on the Nb+Nb dielectron data, the mixed cascade events should adequately represent the real environment. When the impact parameter used in the cascade is restricted to be < 4 fm, the cascade code produces distributions of multiplicities and particle kinematics that are in reasonable agreement with those observed in the spectrometer and the multiplicity array. The resulting total efficiency for these mixed events, as a function of dielectron mass, is shown in Fig. 3. The total efficiency is around 22% for mass values greater than 200 MeV. At lower values, however, the efficiency drops rapidly as the mass decreases. This effect is mostly due to quasitracking cuts that reject two or more particles traversing the same hodoscope element, since low mass pairs and high multiplicity events are both more probable in the elements near the beam. The tracking efficiency $(\epsilon_{\rm tr})$ does not change much with spectrometer multiplicity. The total efficiency is found to be independent of p_t and rapidity.

IV. EXPERIMENTAL RESULTS

The raw data include about 2.7×10^5 triggers (acquired in 40 h of beam time) for Nb+Nb at 1.05 GeV/nucleon. The average flux was 6×10^7 Nb particles per spill and the average live time of the computer about 77%. Offline the raw data are reduced by quasitracking to 7000 events. This reduced set of data are then sent through the full reconstruction code. The number of reconstructed pairs, including opposite and like-sign pairs, at this stage is 469. After sharper time-of-flight and vertex cuts, the final sample reduces to 108 opposite-sign pairs and 54 like-sign pairs giving a number of true pairs of 54 ± 13, $R = T/F = 1.0$ and $T/\sigma_T = 4.2$. The invariant mass distribution of these 54 true pairs is shown in Fig. 4.

The mass-projected differential cross section (which we call the mass spectrum) is obtained by applying the acceptance correction [14], subtracting the like-sign pairs from the opposite-sign pairs, and then summing over the other kinematic variables. This procedure is valid when the number of positive same sign and negative same sign pairs are equal, which is true within the statistics for this experiment. This mass spectrum is shown in Fig. 5. Note that this projected mass spectrum contains only infor-

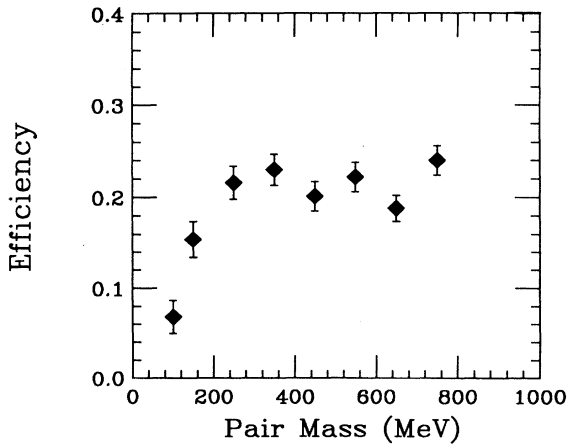

FIG. 3. Efficiency calculated using electron pairs mixed with simulated Nb+Nb hadron events ($b < 4$ fm) vs pair mass.

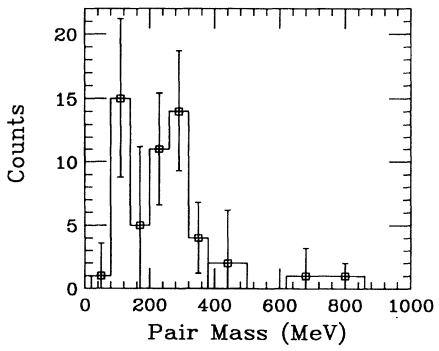

FIG. 4. Mass distribution of the true pairs from the reaction Nb+Nb at 1.05 GeV/nucleon. Events with pair mass below 200 MeV are due mostly to π^0 Dalitz decay.

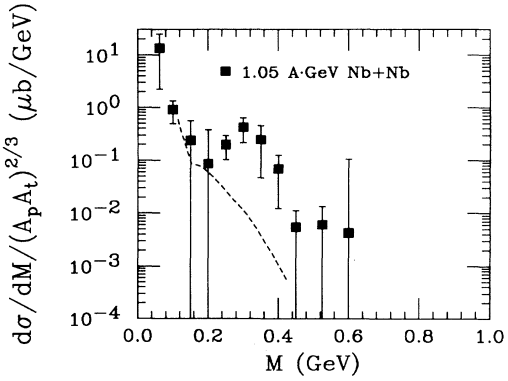

FIG. 5. Dielectron mass spectrum from the reaction Nb+Nb at 1.05 GeV/nucleon with acceptance and efficiency corrections. The dashed curve shows the estimated Dalitz contributions from π^0 and Δ, which is not subtracted.

mation from the cross section within that part of phase space where the DLS apparatus has significant acceptance. A "filter" specifying this multidimensional region must be used to compare theoretical calculations with these measurements. This filter can be obtained from the DLS group. The one-dimensional efficiency correction included in the above mass spectrum is obtained from Fig. 3. An efficiency correction that employs an interpolation of a two-dimensional efficiency table, i.e., $\epsilon(M, N_{sp})$, where N_{sp} is the charge multiplicity in the arms, gives a consistent result. The indicated errors in all figures are only statistical. We estimate, for pairs mass $M < 200$ MeV, less than $^{+40}_{-30}$% systematic error, where the upper limit comes from uncertainty in the correction for the multiplicity effect (< 25%), beam intensity calibration (< 15%), and detection efficiency including a rate dependent trigger efficiency (< 25%). The lower limit is due to corrections for the multiplicity effect and beam intensity calibration. For $M > 200$ MeV, we estimate less than $^{+30}_{-15}$% systematic error with 25% and 15% coming from detection efficiency and beam intensity calibration, respectively, for the upper limit, while the lower limit is due to beam intensity calibration. The dashed curve is our estimated contribution from π^0 and Δ Dalitz decays. These contributions are significant only in the first few mass bins, and are much below the total e^+e^- signal for $M > 250$ MeV.

Figure 6(a) shows the distribution of the number of counts (N_A) in the multiplicity array associated with true pairs having masses greater than 200 MeV (the false pair subtraction was done by the technique indicated above). This distribution peaks at 26. The figure also shows the simulated number of counts in the multiplicity array when the cascade code is run with no restriction on the impact parameter. The shape of this calculated "minimum bias" distribution is similar to the one observed in the experiment if the trigger requirement is that at least one particle passes through the spectrometer. The ratio of the array multiplicity for true pairs to that for the cascade minimum bias data, Fig. 6(b), shows that the e^+e^- pairs are preferentially produced in high multiplicity events. The statistics are too poor to distinguish between a dependence on (N_A) or on $(N_A)^2$.

The limited statistics also precludes a detailed examination of the mass-multiplicity dependence. A rough study was made by dividing the data set into two parts, each with ~20 events, medium mass $180<M<280$ MeV and high mass $M>280$ MeV. The array-multiplicity distributions for each region are shown in Fig. 7. The distributions are observed to be slightly different, with larger mean multiplicities associated with the higher mass bin. Higher statistical precision will be required to confirm this observation.

Following our previous convention, we compare the data sets taken at 1 GeV/nucleon (Nb+Nb, p+Be [12], and Ca+Ca [15]) with each cross section scaled by the factor $(A_pA_t)^{2/3}$. (A_p and A_t refer to the mass number of projectile and target, respectively.) Figure 8(a) shows the mass spectrum for p+Be overlaid with the Nb+Nb result. The curves are our estimates of π^0 and Δ Dalitz contributions for both reactions. Figure 8(b) compares the Ca+Ca and Nb+Nb data sets at 1.05 GeV/nucleon. (Notice that here the first two bins of the Ca+Ca spectrum have been corrected for efficiency loss using the same method as for Nb+Nb.) While the slopes of the p+Be and Nb+Nb spectra are significantly different, the Ca+Ca and Nb+Nb mass spectra are similar in shape.

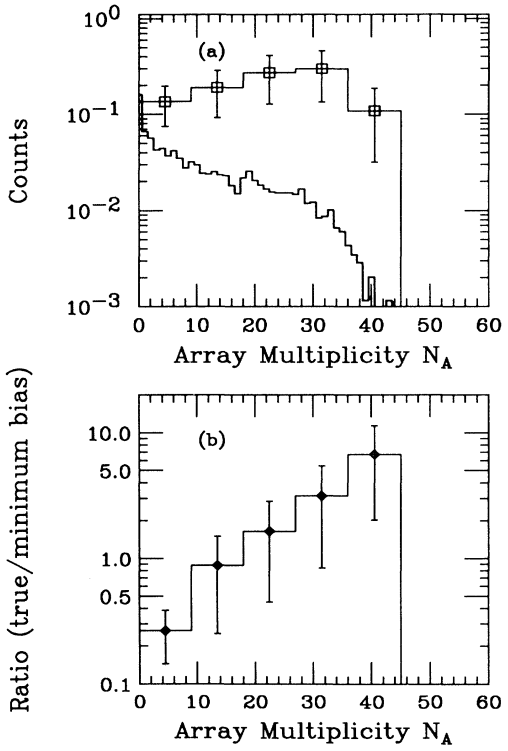

FIG. 6. (a) Multiplicity array hit distribution for true pairs with $M > 200$ MeV in the reaction Nb+Nb (squares). The superimposed spectrum is the cascade minimum bias multiplicity. (b) Ratio of the true pair multiplicity to the minimum bias multiplicity computed from the two histograms above (diamonds).

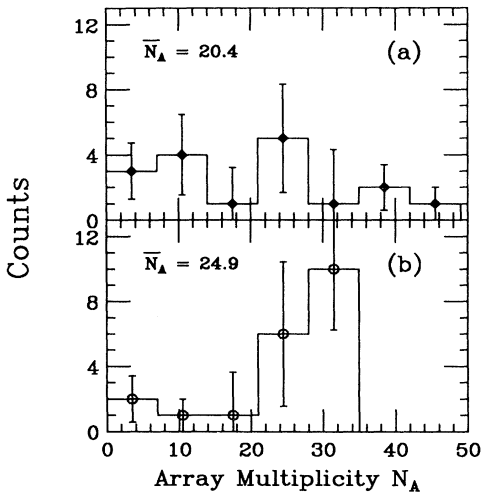

FIG. 7. Distributions of counts in the multiplicity array (N_A) for true pairs from the reaction Nb+Nb for (a) $180 < M < 280$ MeV (diamonds) and (b) $M > 280$ MeV (circles). The mean multiplicity ($\overline{N_A}$) is also indicated for each mass cut.

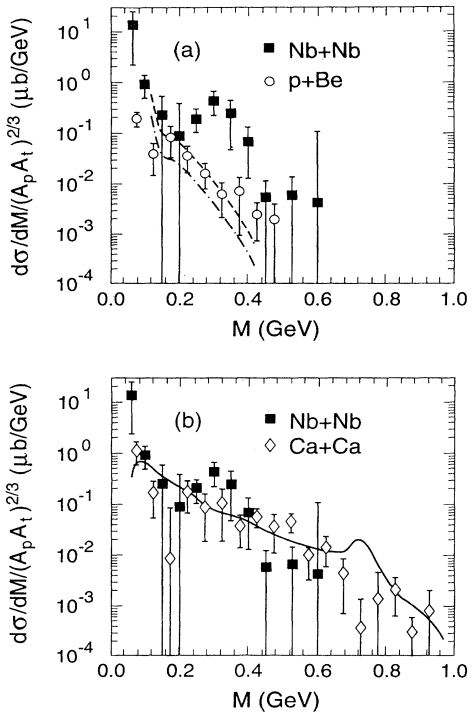

FIG. 8. (a) Comparison of Nb+Nb (squares) with p+Be (circles) collisions at 1.05 GeV/nucleon. The dashed and dot-dashed curves are the estimated π^0 and Δ Dalitz contributions for Nb+Nb and p+Be, respectively. (b) Comparison of Nb+Nb (squares) with Ca+Ca (diamonds) collisions at the same energy. The solid curve is from a calculation by Xiong *et al.* including contributions from pn bremsstrahlung, delta decay, pion absorption by nucleon, and $\pi\pi$ annihilation [16].

The solid curve in Fig. 8(b) shows the result from a calculation done by Xiong *et al.* [16], which is in general agreement with the data except for the lowest and highest masses. Note, however, that the DLS experimental resolution was not included in the theoretical result, which can perhaps explain the discrepancy in the ρ-ω region. Calculations based on this model and others [17, 18] indicate a sizable contribution from $\pi^+\pi^-$ annihilation for masses greater than 400 – 500 MeV [17, 18].

The dependence of cross sections on the number of nucleons in the projectile (A_p) and in the target (A_t) has been found to provide information about the interactions that produce the observed final state [19–21]. Rescattering (multiple interactions) of either the incident particles or the produced secondaries is of particular interest in determining the amount of collectivity present during the collision. For the interactions of single particles with nuclear targets, the dependence is frequently parametrized as $\sigma \propto A_t^\alpha$. This idea may be extended to the case of nucleus-nucleus interactions by using the parametrization $\sigma \propto (A_pA_t)^\alpha$. (A particular value of α may have different meanings for these two cases.)

The DLS mass spectra have been integrated above 200 MeV for the three reactions measured at 1.05 GeV/nucleon. The lower mass limit was chosen to exclude the yield from pi-zero Dalitz decays. These integrated cross sections are plotted vs (A_pA_t) in Fig. 9. The error bars are statistical and the brackets indicate our estimate of systematic errors. Fitting the Ca+Ca and Nb+Nb data with the parametrization $(A_pA_t)^\alpha$, we find $\alpha = 1.0 \pm 0.27$. This result is larger than, but not significantly different from, the value of 2/3 to be expected if the pairs are produced by collisions between two nucleons neither of which has had a previous inelastic collision. Secondary nucleon collisions are unlikely to directly pro-

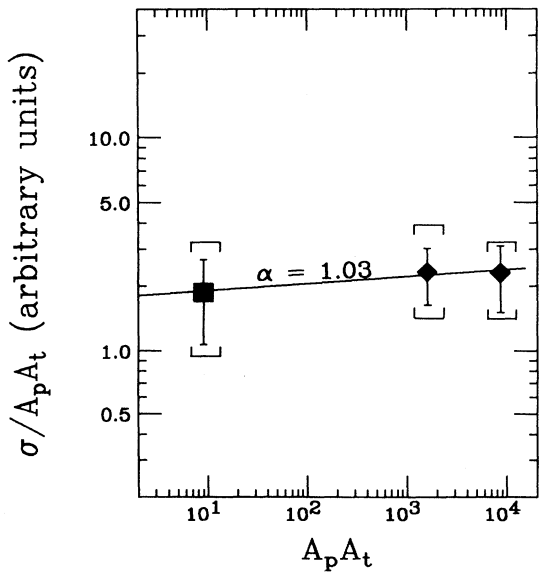

FIG. 9. Integrated cross sections (nanobarns) at 1.05 GeV/nucleon, for $M \geq 200$ MeV, normalized by A_pA_t, and a straight line showing $\alpha = 1.03$.

duce electron pairs above the lower limit to the integration because the integrated pair-production cross section is decreasing rapidly with decreasing Q (available energy in the NN center of mass) [12].

The contribution to Q from Fermi motion is smaller for the p+Be data set than for the Ca+Ca and Nb+Nb data sets because of the absence of Fermi motion in the projectile. When coupled with the strong Q dependence of the pair yield this suggests that comparisons between the three data sets may not be simply interpretable. We note for the record that a fit of the parametrization $(A_pA_t)^\alpha$ to the three data sets yields $\alpha = 1.03 \pm 0.03$. The small error bar on this fitted value reflects the larger lever arm in (A_pA_t) offered by the p+Be data.

V. CONCLUSION

We have measured the cross sections for the reaction Nb+Nb$\rightarrow e^+e^-+X$ at 1.05 GeV/nucleon. A multiplicity array was used to measure the associated charged particle multiplicity. This first report of a cross section for dielectron production for this projectile/target combination establishes the feasibility of such experiments. The mass resolution of the spectrometer is not greatly affected by the high multiplicity environment, but the efficiency of detecting e^+e^- pairs in the low mass region, $M < 200$ MeV, is reduced by increased multiplicity. The contributions from Dalitz decays of π^0 and Δ are estimated to be below the observed cross section and are only significant in the mass region M <150 MeV. A comparison with simulation indicates that the electron pairs result from central collisions with impact parameters $b < 4$ fm. Finally, the dielectron cross section is found to be consistent with a linear dependence on A_pA_t.

ACKNOWLEDGMENTS

This work was supported by the Office of Energy and Research, Office of High Energy and Nuclear Physics, Nuclear Physics Division of the U.S. Department of Energy under Contracts Nos. DE-AC03-76SF00098, DE-FG03-88ER40424, DE-FG02-88ER40413, and DE-FG05-88ER40445. We thank the LBL engineering and Bevalac operation staff for their continued support of this project.

[1] L.P. Csernai and J.I. Kapusta, Phys. Rep. **131**, 223 (1986).
[2] H. Stöcker and W. Greiner, Phys. Rep. **137**, 277 (1986).
[3] G.F. Bertsch and S. Das Gupta, Phys. Rep. **160**, 189 (1988).
[4] C. Gale and J. Kapusta, Phys. Rev. C **40**, 2397 (1989).
[5] C. Gale and J. Kapusta, Phys. Rev. C **35**, 2107 (1987).
[6] L.H. Xia *et al.*, Nucl. Phys. **A485**, 721 (1988).
[7] G. Roche *et al.*, Phys. Rev. Lett. **61**, 1069 (1988).
[8] A. Yegneswaran *et al.*, Nucl. Instrum. Methods A **290**, 61 (1990).
[9] J. Cugnon, T. Mizutani, and J. Vandermeulen, Nucl. Phys. **A352**, 505 (1981); J. Cugnon, J. Knoll, and J. Randrup, *ibid.* **A360**, 444 (1981); J. Cugnon, *ibid.* **A387**, 524 (1982).
[10] J.S. Gordon, Ph.D. thesis, University of California, Los Angeles, 1989.
[11] M. Cahay, J. Cugnon, and J. Vandermeulen, Nucl. Phys. **A411**, 524 (1983).
[12] C. Naudet *et al*, Phys. Rev. Lett. **62**, 2652 (1989).
[13] S. Y. Beedoe, Ph.D. thesis, University of California, Los Angeles, 1991.
[14] A. Letessier-Selvon *et al.*, Phys. Rev. C **40**, 1513 (1989).
[15] G. Roche *et al.*, Phys. Lett. B **226**, 228 (1989).
[16] L. Xiong *et al.*, Nucl. Phys. **A512**, 772 (1990).
[17] Gy. Wolf *et al.*, Nucl. Phys. **A517**, 615 (1990); Gy. Wolf *et al.*, Phys. Rev. C **43**, 1501 (1991).
[18] L. Winckelmann *et al.*, GSI Scientific Report 1990 (1990), p. 103.
[19] S. Nagamiya *et al.*, Phys. Rev. C **24**, 971 (1981).
[20] W. Geist, Nucl. Phys. **A525**, 149c (1991).
[21] A. Capella, Nucl. Phys. **A525**, 133c (1991).